Journal of Catalysis **187,** 367–384 (1999)
Article ID jcat.1999.2641, available online at http://www.idealibrary.com on IDEAL®

Preparation and Characterization of Supported Bimetallic Pt–Au Particle Catalysts from Molecular Cluster and Chloride Salt Precursors

Bert D. Chandler, Alexander B. Schabel, Christopher F. Blanford, and Louis H. Pignolet[1]

Department of Chemistry, University of Minnesota, 207 Pleasant Street SE, Minneapolis, Minnesota 55455

Received February 22, 1999; revised July 14, 1999; accepted July 15, 1999

New silica-supported bimetallic Pt–Au catalysts were prepared using an organometallic Pt–Au cluster precursor and compared with Pt and Pt–Au catalysts prepared by the incipient wetness impregnation of chloride salts. The supported catalyst precursors were calcined and reduced under identical conditions and the resulting catalysts were characterized with transmission electron microscopy (TEM), energy-dispersive spectroscopy (EDS), CO chemisorption, and diffuse reflectance infrared Fourier Transform spectroscopy (DRIFTS). Temperature-programmed reduction experiments were also performed on the freshly supported precursors and after calcination. The bimetallic cluster precursor yielded catalysts with small ($d \approx 2.5$ nm), uniform particles that have high Pt dispersion. EDS, CO chemisorption, and DRIFTS of adsorbed CO experiments gave strong evidence that these particles are bimetallic. Using the organometallic cluster precursor also caused a significant red shift (12 cm^{-1}) in the stretching frequency of adsorbed carbon monoxide relative to the traditional Pt catalyst. Catalytic performance was evaluated with the hexane conversion reaction. Results showed that the cluster-derived catalysts enhance the production of light hydrocarbons and decrease the rate of skeletal reforming reactions. Despite the enhancement of C–C bond fission reactions, catalysts prepared from the organometallic precursor had greatly enhancing resistance to deactivation. In contrast, the coimpregnation of Au with Pt from chloride salts yielded catalysts with little or no interaction between the two metals. For these catalysts, light hydrocarbon production decreased yet skeletal rearrangements were not measurably affected.

Key Words: **platinum; gold; Pt clusters; bimetallic catalysts; molecular precursors; hexane conversion; hydrogenolysis; cracking; alkane reforming.**

INTRODUCTION

Since the development of "platforming" processes in the late 1940s and the later discoveries that Pt catalyzes alkane skeletal rearrangement reactions, Pt-based catalysts have been extensively studied for many applications. Supported Pt catalysts, often with a second metal or other dopants added, are currently being examined as emissions control catalysts and are the mainstay for alkane conversion catalysts in the petrochemical industry (1, 2). Recent discoveries that very small Pt particles or clusters on basic supports catalyze the formation of aromatics from alkanes with excellent selectivity have also sparked a great deal of research into the area of supported Pt catalysts. The addition of gold to platinum-based alkane conversion catalysts is of particular interest. Gold by itself is catalytically inactive for alkane reforming reactions below 400°C (3, 4) and the study of Pt–Au catalysts has afforded the opportunity to study the importance of geometric effects on catalysis by Pt.

Bulk and supported Pt–Au alloys (average particle diameter >10 nm) have been extensively studied as catalysts for reactions of alkanes and cycloalkanes (4–11). Although specific results are varied in the literature, certain conclusions are generally agreed on for bulk and supported alloys: (1) Au acts as a diluent breaking up large Pt ensembles and (2) alloy activities and selectivities for alkane reforming are greatly affected by the Au content of the alloy. As the Au content of the alloy increases, the number of large Pt ensembles decreases and the number of small ensembles increases. The smallest ensembles are often described as small islands of Pt or even single Pt atoms in a sea of Au. As the relative numbers of large and small ensembles change on these single-crystal alloys, the associated changes in reforming selectivity have been used to rationalize particle size effects for supported Pt catalysts. Temperature-programmed desorption (TPD) of H_2 and CO studies have been used to examine the relative contributions of electronic (ligand) and geometric effects for these alloys. Generally, ligand effects are considered to be small and observed differences in catalysis are explained on the basis of geometric and ensemble size arguments.

Studies of Pt–Au films (4, 12) and alloyed single crystals (8, 10, 12) similarly explain catalysis results in terms of geometric arguments. They also provide an additional and important insight into the complexity of structure sensitivity for bimetallic systems. Studies annealing Au on Pt(100) and Pt(111) single crystals indicate that *n*-hexane conversion is greatly affected by the gold content of the resulting alloy, in

[1] To whom correspondence should be addressed. Fax: (612) 626–5741. E-mail: pignolet@chem.umn.edu

0021-9517/99 $30.00

good agreement with the aforementioned results for supported alloys. They also show that the crystal face on which catalysis occurs has a pronounced effect on both activity and product selectivity (8, 10). As expressed by the authors (10), this might account for the wide array of seemingly disparate catalysis results in the literature for supported Pt–Au catalysts.

Recent research on bimetallic Pt-based catalysts has focused on the preparation and characterization of supported bimetallic particle catalysts with average particle diameters <10 nm, rather than supported alloys. Most of the efforts in preparing and characterizing supported Pt–Au catalysts have been limited to the coimpregnation of Pt and Au salts such as platinic and auric acids (11, 13–17). Phase separation is a common problem with this method because Pt–Au alloys between 18 and 97% Pt are not thermodynamically stable (18). In addition, such wetness impregnation techniques often yield catalysts with wide ranges of particle sizes and compositions and varying degrees of metal interaction (11).

A different approach to the preparation of supported metal particle catalysts is to adsorb organometallic precursors (particularly molecular cluster compounds) intact on the support and thermally remove the ligands. Past studies in this field have largely involved the use of mono- and bimetallic carbonyl clusters as precursors (19–29). In these studies, molecular cluster compounds were supported on various oxide supports (e.g., silica, alumina, magnesia, zeolites) and subsequently decarbonylated by heating under vacuum or an inert atmosphere. Further studies have shown that in some cases the structure of the metal core remains substantially intact after ligand removal (27–29). These well-defined metal cluster catalysts have been examined with a variety of probe reactions, the results of which have important implications for the nature of catalytic active sites (27–29).

Unfortunately, clusters containing both platinum and gold that are ligated exclusively by CO are not available; however, there are many molecular Pt–Au clusters stabilized by phosphine ligands (30–32). Some of these phosphine-stabilized clusters have been supported and thermalized to obtain metal particle catalysts in previous studies (33–36). Results of these studies indicated that the presence of phosphine residues controls the properties of these catalysts and efficiently poisons alkane reforming reactions. At the same time, the hydrogenation and dehydrogenation activity of these catalysts are relatively unaffected by the presence of phosphorus and these catalysts may find utility as selective dehydrogenation catalysts (36, 37).

Because of the dominance of phosphorus effects when phosphine-stabilized clusters are used as catalyst precursors, in the current study Pt–Au catalysts are derived from a bimetallic cluster ligated exclusively by acetylide ligands. The $Pt_2Au_4(C{\equiv}C^tBu)_8$ cluster is an ideal candidate for the preparation of supported Pt–Au catalysts. It is one of the few known Pt–Au compounds stabilized by ligands that contain only carbon and hydrogen and the Pt and Au atoms in the cluster are in lower oxidation states (II and I, respectively) than in chloride salts. Not only does the cluster dissolve and remain intact in a variety of organic solvents (38), but it quickly and spontaneously adsorbs onto silica from hexane solution. In addition, this cluster contains Pt and Au in a ratio that falls outside the miscibility range for traditional Pt–Au alloys, offering the possibility of preparing bimetallic particle catalysts of unique metal composition and morphology.

METHODS

Catalyst preparation. The organometallic cluster $Pt_2Au_4(C{\equiv}C^tBu)_8$ was prepared from $[N(C_4H_9)_4]_2[Pt(C{\equiv}C^tBu)_4]$ and $Au(C_4H_8S)Cl$ via published procedures (38). Hexachloroplatinic acid, $H_2PtCl_6 \cdot 6H_2O$, was prepared from Pt metal (99.99%) according to a published procedure (39). Auric acid ($HAuCl_4 \cdot H_2O$) was purchased from Strem. Davisil SiO_2 (35–60 mesh, BET surface area = 360 m^2/g, average pore diameter = 150 Å) was washed with high-purity Millipore distilled and deionized water to remove the fine particles and dried under vacuum at 120°C for 24 h prior to use. Conventional Pt and Pt–Au catalysts were prepared by incipient wetness impregnation and coimpregnation of the chloride precursors onto the dried silica support. Solution concentrations were adjusted to give the following catalysts: 1-Pt (1% Pt), Au (2% Au), 1-(Pt + 2Au) (1% Pt + 2% Au), 0.15-Pt (0.15% Pt), 0.15-(Pt + 2Au) (0.15% Pt + 0.3% Au). The abbreviations indicate Pt weight percentage and atomic Pt–Au ratio of the precursors. Abbreviations are used only to refer to catalysts that have undergone the standard activation protocol (see below). The bimetallic cluster $Pt_2Au_4(C{\equiv}C^tBu)_8$ spontaneously adsorbed onto silica from hexane solution. The details of the general procedure have been previously reported for the support of phosphine-stabilized Pt and Pt–Au compounds (33, 37). The resulting catalyst loadings and abbreviations are 1-Pt_2Au_4 (1% Pt, 2% Au) and 0.15-Pt_2Au_4 (0.15% Pt, 0.3% Au).

Temperature-programmed reduction. In temperature-programmed reduction (TPR) experiments, 200 mg of the supported precursor was placed into the quartz microreactor and attached to the RXM-100. Argon gas from the reference side of the TCD detector (operated at 80 mV) was used to purge the sample; the effluent gas was passed through a dry ice/acetone bath before entering the sample side of the detector. After the detector baseline had stabilized, the detector was briefly turned off and the gas was switched to 1% H_2 in Ar. After 3–5 min, the detector was turned on and the baseline allowed to stabilize. The sample temperature was then ramped 15°C/min to 700°C while

the detector response was monitored with an interfaced Macintosh computer running software from Advanced Scientific Designs, Inc. For the TPR of the oxidized precursors, the samples were loaded into the microreactor, attached to the RXM-100, and oxidized at 300°C for 2 h (see above). After 2 h of oxidation, the flowing gas was switched to Ar flowing at 100 mL/min, the sample was cooled to 30°C under Ar flow, and the TPR protocol (as above) was followed.

Chemisorption experiments. All adsorption isotherms were measured at 20°C over an equilibrium pressure range of 10–60 Torr. The chemisorption protocol was as follows. Following catalyst pretreatment, samples were cooled 10°C/min under flowing H_2 to 135°C and evacuated for 20–60 min, until a base pressure of 1×10^{-6} was reached. The samples were then cooled to room temperature under high vacuum and the furnace was replaced with a water bath. A CO uptake isotherm was measured at 22 ± 2°C, the sample was then evacuated at this temperature for 10 min, and a second CO uptake isotherm was measured. Total CO chemisorption was determined by subtracting the physical adsorption isotherm of CO on a silica blank that had undergone the identical standard activation and chemisorption protocols. The strongly bound CO isotherm was determined by subtracting the second measured CO uptake isotherm from the first. The weakly bound CO is the difference between the total CO chemisorption and the strong CO chemisorption. All chemisorption calculations were done using Advanced Scientific Designs, Inc. software. For the CO chemisorption experiments, the dispersion ($Pt_{surface}/Pt_{total}$) is equal to the ratio of adsorbed CO to total platinum atoms (CO/Pt_{total}) calculated from the total and strong CO uptake isotherms at 60 Torr on catalyst samples assuming a CO : Pt adsorption stoichiometry of 1 : 1 (40).

Diffuse reflectance infrared Fourier transform spectroscopy (DRIFTS). DRIFTS studies were conducted with a Magna 750 FTIR system (Nicolet) using a DRIFTS cell (SpectraTech) equipped with a SpectraTech accessory that allows *in situ* treatments with different gases at temperatures up to 900°C. OMNIC software was used for data processing. A liquid nitrogen-cooled MCT detector was used for data collection. The interferograms consisted of 512 scans and the spectra were collected with a 2 cm^{-1} resolution in the absorbance format using a KBr spectrum as the background. The silica-supported precursors were pretreated by the standard activation protocol on the RXM-100 system. In some cases they had been previously used in standard hexane conversion experiments (see below). The samples were finely ground with an agate mortar and pestle (important) and placed into the DRIFTS cell where they were rereduced under a flow of H_2 at 200°C and ambient pressure. After reduction, the samples were cooled under flowing nitrogen and a spectrum was recorded. The samples were then treated with carbon monoxide at room temperature and ambient pressure by flowing CO through the cell for 1.5 min. The cell was then flushed with nitrogen for 5 min and a spectrum was collected. To best observe the peaks corresponding to bound CO, the spectra collected before CO treatment were subtracted from the spectra after CO treatment.

Transmission electron microscopy (TEM) and energy-dispersive spectroscopy (EDS). Samples were prepared for TEM by first crushing them with an agate mortar and pestle, then dispersing about 20 mg of the powder in 2 mL 1,2-dichloroethane by ultrasonification for 30 min. Five drops of the suspension was then dripped onto a holey carbon grid. Samples were examined by transmission electron microscopy (TEM) using a Philips CM30 transmission electron microscope equipped with a LaB_6 or W filament running at 300 kV. Images were recorded on photographic film and scanned with a Microtech ScanMaker III before further analysis. Energy-dispersive spectra were recorded using an attached EDAX PV9900 energy-dispersive spectrometer. Spectra were typically recorded for 200-s live time with the sample tilted 30° toward the detector. Particles were measured from TEM images using NIH Image 1.61 PPC software. Individual particles were measured in three different directions and the average was used as the particle diameter. Particle size distributions were prepared from at least three different photomicrographs (magnification usually $\geq$200 kX) using at least 100 particles.

Hexane conversion. A saturated hexane (Aldrich Chemical Co., 99+%)-in-hydrogen gas stream was produced with a two-stage hexane bubbler apparatus through gas dispersion frits. The second stage was submerged in an ice bath to maintain a hydrogen : hexane ratio of 16 : 1 (partial pressure of hexane = 49 Torr). The gas mixture was fed directly to the RXM-100 reaction manifold where it subsequently flowed over the catalyst bed. The catalysis runs were all conducted at 400°C. The weight hourly space velocity [WHSV = (g hexane in feed)(g Pt)$^{-1}$(h^{-1})] of hexane was typically between 2 and 20 h^{-1}. Reaction products were analyzed on stream via gas chromatography using a Hewlet–Packard 5890A gas chromatograph operated with a flame ionization detector. Product separation was achieved with use of a 30-ft SP-1700-coated 80/100 Chromosorb P AW-packed column (Supelco) operated at 85°C and column head pressure of 100 psi. Products were identified by calibrating peak retention times with known hydrocarbons. The products were classified into five categories: cracking (formation of C_1–C_5 hydrocarbons), isomerization (2-methyl- and 3-methylpentane), hexenes, methylcyclopentane (MCP), and 1,6-cyclization (cyclohexane and benzene). Yields of products were measured in mass percentages, and were corrected for impurities in the hexane feed. Blank runs with plain SiO_2 and Au showed no activity under reaction conditions.

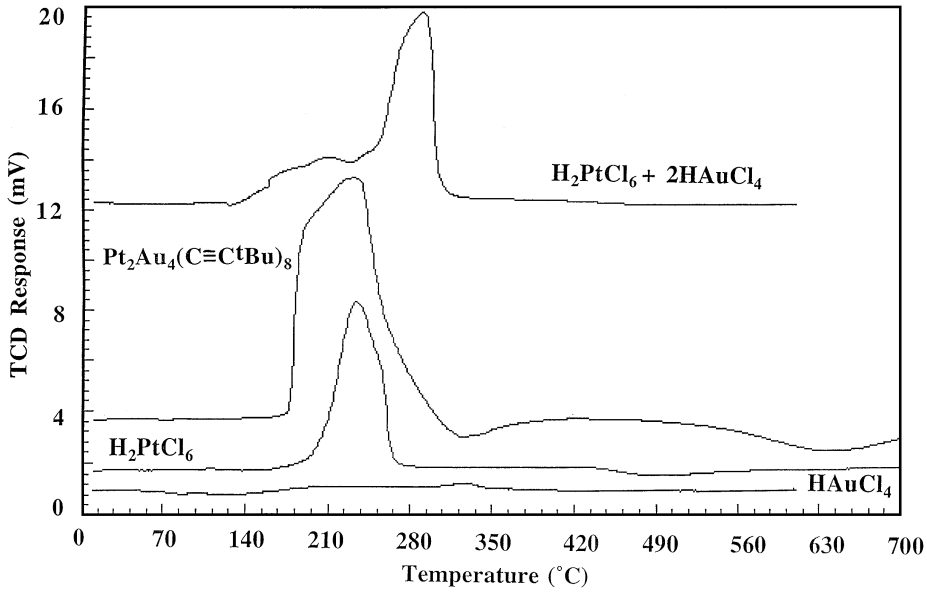

FIG. 1. Temperature-programmed reduction profiles of the freshly supported precursors. All metal loadings are 1% Pt and 2% Au.

RESULTS

A series of silica-supported platinum and platinum–gold catalysts was prepared to study the effects of gold and precursor type on catalyst activity, selectivity, and structure. The three types of catalysts used in this study [Pt, Pt, and Au from chloride salts, and Pt and Au from the $Pt_2Au_4(C{\equiv}C^tBu)_8$ cluster] were each studied at 1 and 0.15 wt% Pt on silica. To make reasonable comparisons between the traditional wetness-coimpregnated catalysts and the catalysts derived from the molecular precursor, the Pt : Au ratio was 0.5 for all bimetallic catalysts and activation protocols were identical for all catalysts. Activation conditions were chosen to be as mild as possible based on temperature-programmed oxidation experiments, which indicated that ligand oxidation of the supported $Pt_2Au_4(C{\equiv}C^tBu)_8$ cluster occurs primarily between 170 and 250°C.

Temperature-Programmed Reduction

TPR experiments were performed on the supported (nonactivated) precursors and after the oxidation step. Figures 1 and 2 show the TPR profiles for the 1% loaded catalysts. Profiles for the 0.15% Pt catalysts are qualitatively

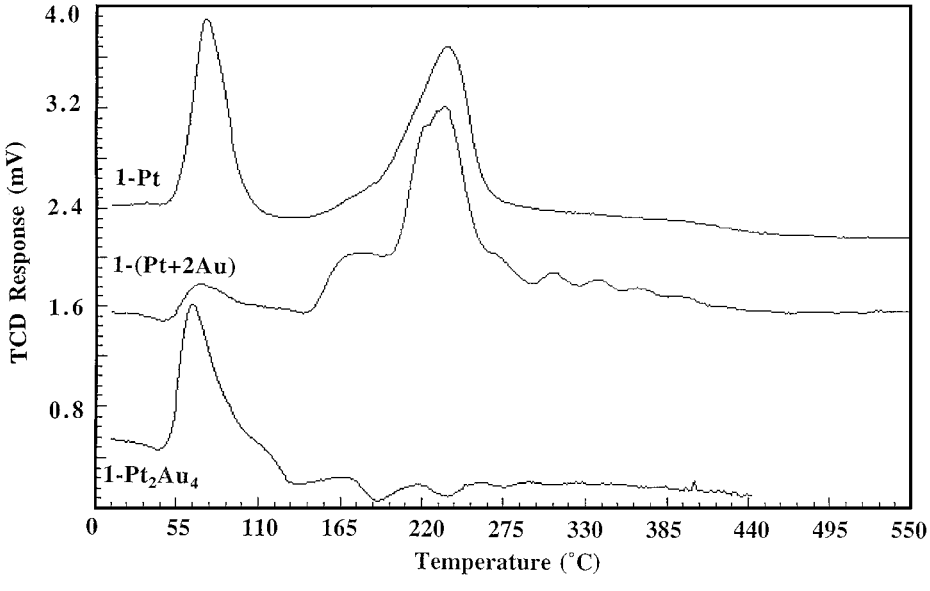

FIG. 2. Temperature-programmed reduction profiles of the oxidized precursors.

similar and are not shown. Reduction of platinic acid (H_2PtCl_6) on silica is observed as a large single reduction peak centered at 235°C, in excellent agreement with data reported in the literature (11). We do not observe comparably large hydrogen uptake peaks for supported auric acid ($HAuCl_4$); the hydrogen uptake of 2% auric acid on silica is roughly 15 to 20 times smaller than that of any of the platinum-containing catalysts. This profile is best described as a gradual reduction that begins at approximately 130°C and continues throughout the course of the experiment. The initial uptake maximizes at 220°C and a second peak occurs at 325°C.

The TPR profile of the freshly coimpregnated platinic and auric acid catalyst is significantly different from that of either of the monometallic profiles. There is an initial reduction beginning at 132°C and peaking at 207°C. This peak greatly resembles the initial reduction of auric acid, but is associated with a much larger uptake of hydrogen than is observed for $HAuCl_4$ on silica. The primary reduction peak that is most similar in shape and size to platinic acid is shifted 55°C higher. Similar observations have been reported for these salts supported on silica, although not at the specific Pt : Au ratio of 0.5 (11). Using the molecular precursor $Pt_2Au_4(C{\equiv}C^tBu)_8$ as the source of both metals gives a single reduction peak that begins at 175°C, is centered at roughly 210°C, and has a maximum signal at 232°C. This peak is significantly larger than the platinic acid peak.

After the oxidation step of the standard activation protocol (flowing O_2 at 300°C for 2 h) there are significant differences in the hydrogen uptake profiles for all of the catalysts. Oxygen-pretreated platinic acid (Fig. 2) has two reduction peaks. The first (75°C) is consistent with the reduction of a Pt oxide or oxychloride (41) and the second (236°C with a shoulder at ca. 180°C) corresponds to the reduction of unoxidized platinic acid. The codeposited platinic and auric acid catalyst resembles platinic acid after the oxidation step. There is a small peak at 73°C from a platinum oxide and a large peak at 234°C associated with platinic acid reduction. There is also a peak at 175°C that coincides with the shoulder on the platinic acid peak. We do not observe large reduction peaks for oxidized 2% $HAuCl_4$ on silica. The reduction profiles of the catalysts derived from the molecular precursor are quite different. There is a single hydrogen uptake peak at 65°C.

Transmission Electron Microscopy

To evaluate metal particle size, TEM experiments were performed on catalyst samples after the standard activation protocol and after hexane conversion catalysis. Figures 3, 4, and 5 contain the histograms of particle size distributions measured from TEM images for all the catalysts after the standard activation protocol. Particle size distributions for catalysts that had been used in the hexane conversion reaction were not significantly different from

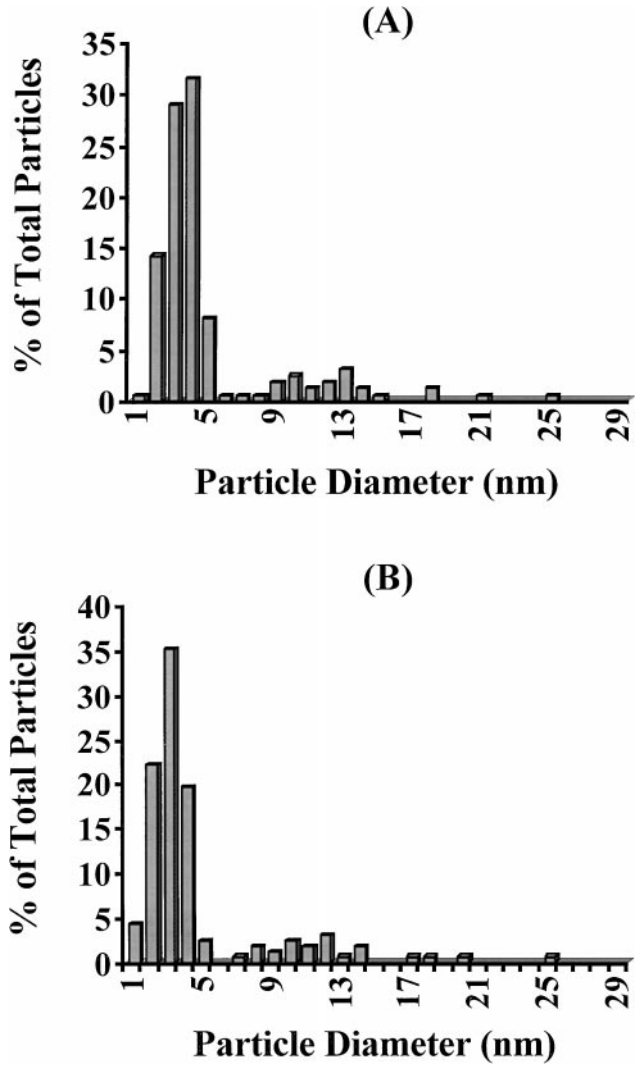

FIG. 3. Particle size distributions for the (A) 1-Pt and (B) 0.15-Pt catalysts.

those of the activated catalysts and are not shown. Results for the 1-Pt, 1-(Pt + 2Au), 0.15-Pt, and 0.15-(Pt + 2Au) catalysts are consistent with previously reported results for wetness-impregnated and -coimpregnated Pt catalysts (1). Not all of the silica particles contained Pt [confirmed by energy-dispersive spectroscopy (EDS)]; i.e., the metal was inhomogeneously distributed through the support particles. For the 0.15-Pt and 1-Pt catalysts, particle size is largely independent of metal loading. Roughly 60% of the observed particles were smaller than 3.5 nm and both catalysts have average particle sizes (determined from TEM images) of about 4.5 nm.

Silica particles containing no metal were often found for the 0.15-(Pt + 2Au) and 1-(Pt + 2Au) catalysts, indicating that the Au containing wetness-coimpregnated catalysts was also inhomogeneously distributed on the support. In addition, the two metals appear to be severely phase

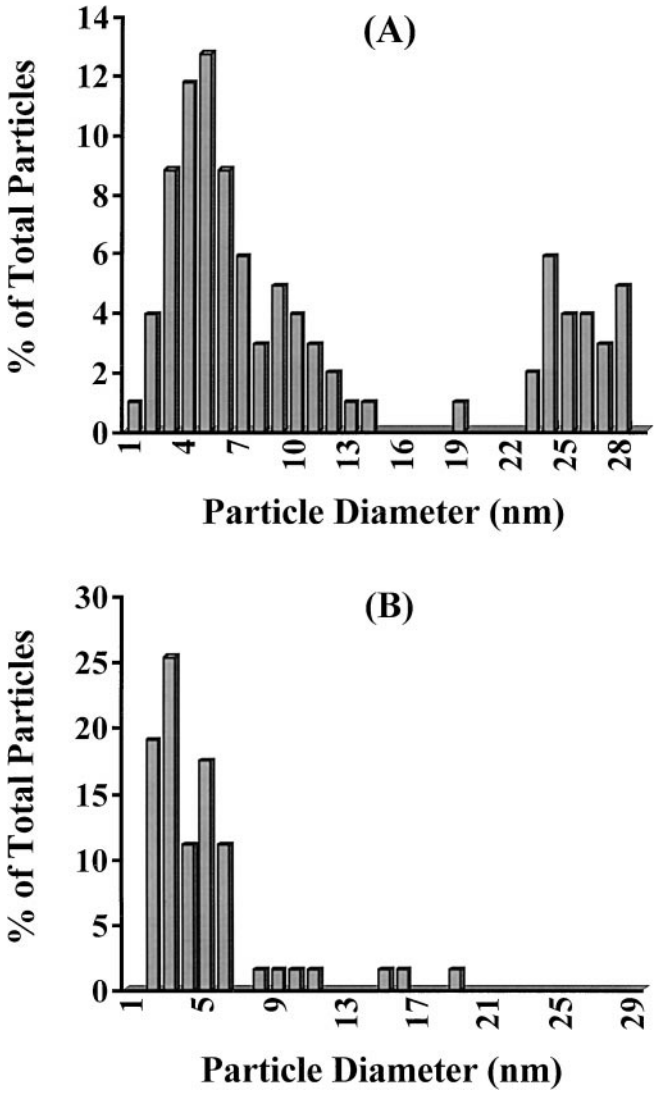

FIG. 4. Particle size distributions for the (A) 1-(Pt + 2Au) and (B) 0.15-(Pt + 2Au) catalysts. Note: Observed particles with diameters >80 nm (>98% Au) are not included.

separated. In many cases, extremely large (ca. 100-nm-long) particles were imaged and determined to be ≥98% Au by EDS. For both catalysts, the energy-dispersive spectra changed significantly depending on the particle sizes present in the region being examined. Regions containing predominantly large particles (≥10 nm) were enriched in Au while regions containing only small particles (<4 nm) were found to contain primarily Pt. Regions containing both large and small particles varied in metal composition. Energy-dispersive spectra of silica particles that contained metal showed an approximate Pt : Au ratio of 1 : 2.

Micrographs of the Pt_2Au_4 catalysts, such as the one shown in Fig. 6, are very different from those of traditionally prepared bimetallic catalysts. Figure 6 also includes an energy-dispersive spectrum from this particle using a probe diameter of roughly 100 nm. For both Pt_2Au_4 catalysts, small and much more uniform particles were imaged in thin sections of the support as indicated by the histograms in Fig. 5. Roughly 90% of the observed particles were smaller than 3.5 nm and both catalysts have average observed particle sizes of around 2.5 nm. The metal particles were too small to collect energy-dispersive spectra of individual particles; however, spectra from regions of silica containing several particles confirmed the presence of both Pt and Au in an approximate ratio of 1 : 2. The exceptionally large particles ($d \approx 100$ nm) observed in the coimpregnated chloride salt catalysts were never observed when the bimetallic cluster was used as the catalyst precursor.

CO Chemisorption and DRIFTS of Adsorbed CO

Platinum availability at room temperature was measured by CO chemisorption and diffuse reflectance infrared

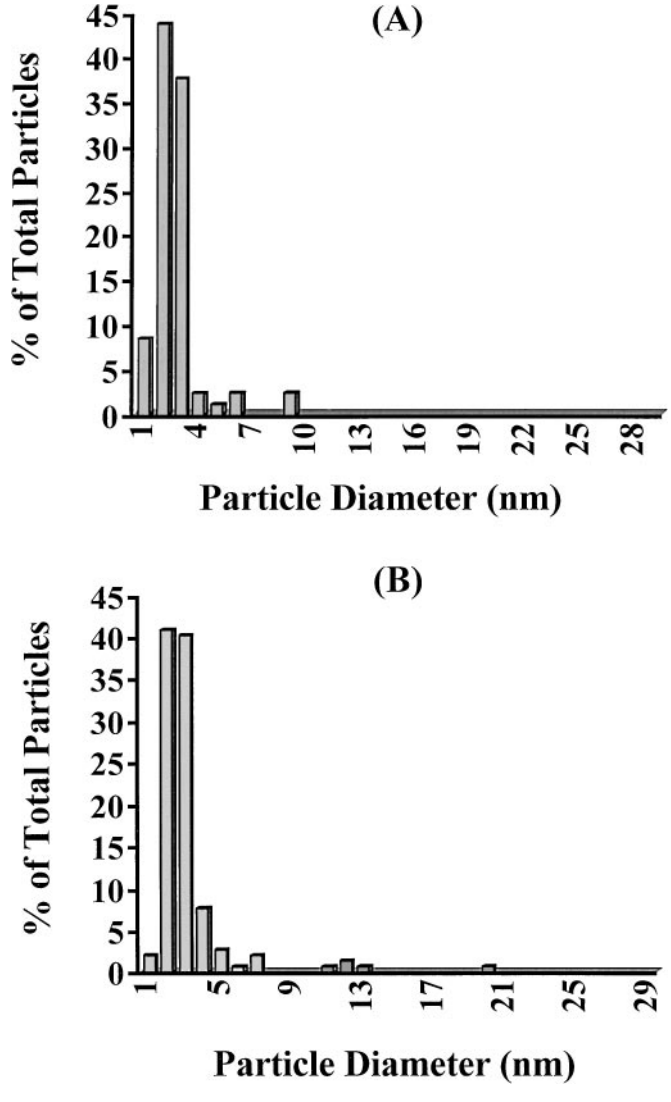

FIG. 5. Particle size distributions for the (A) 1-Pt_2Au_4 and (B) 0.15-Pt_2Au_4 catalysts.

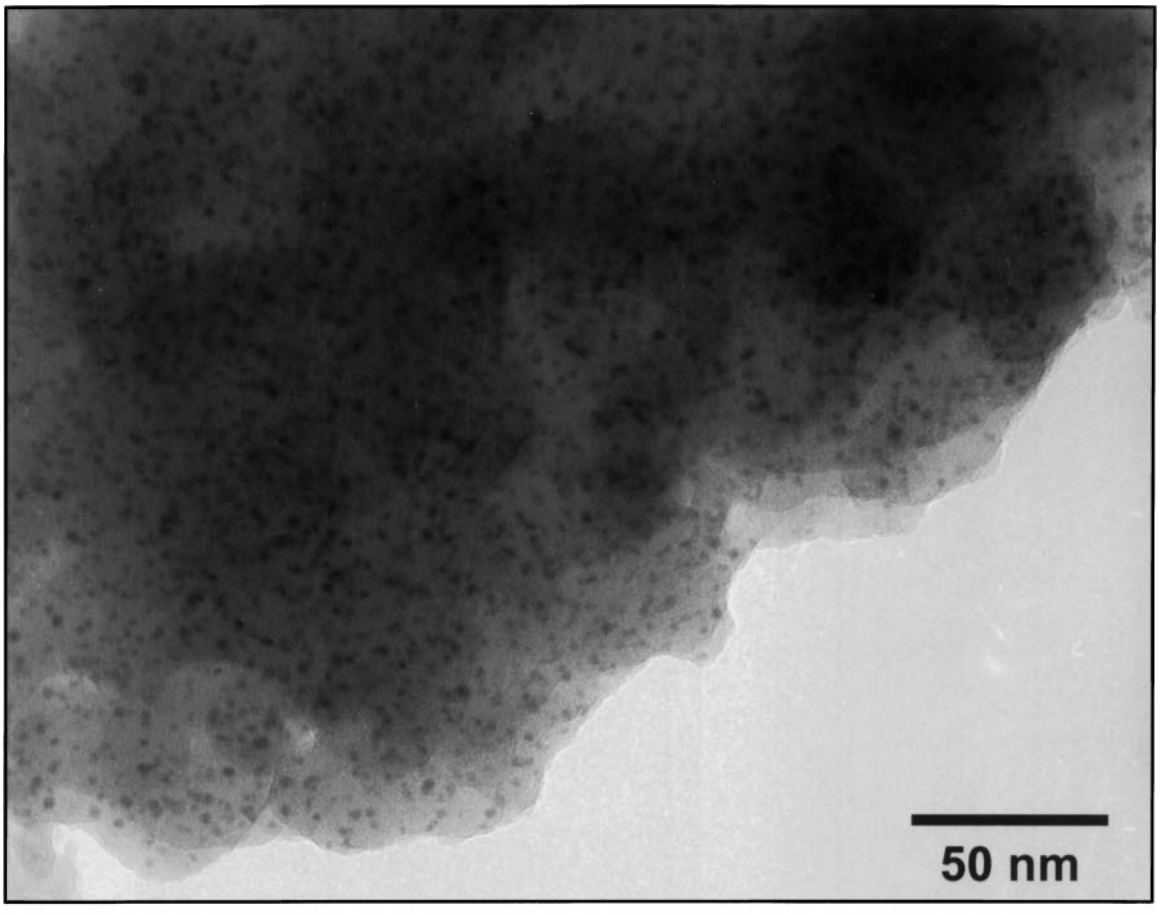

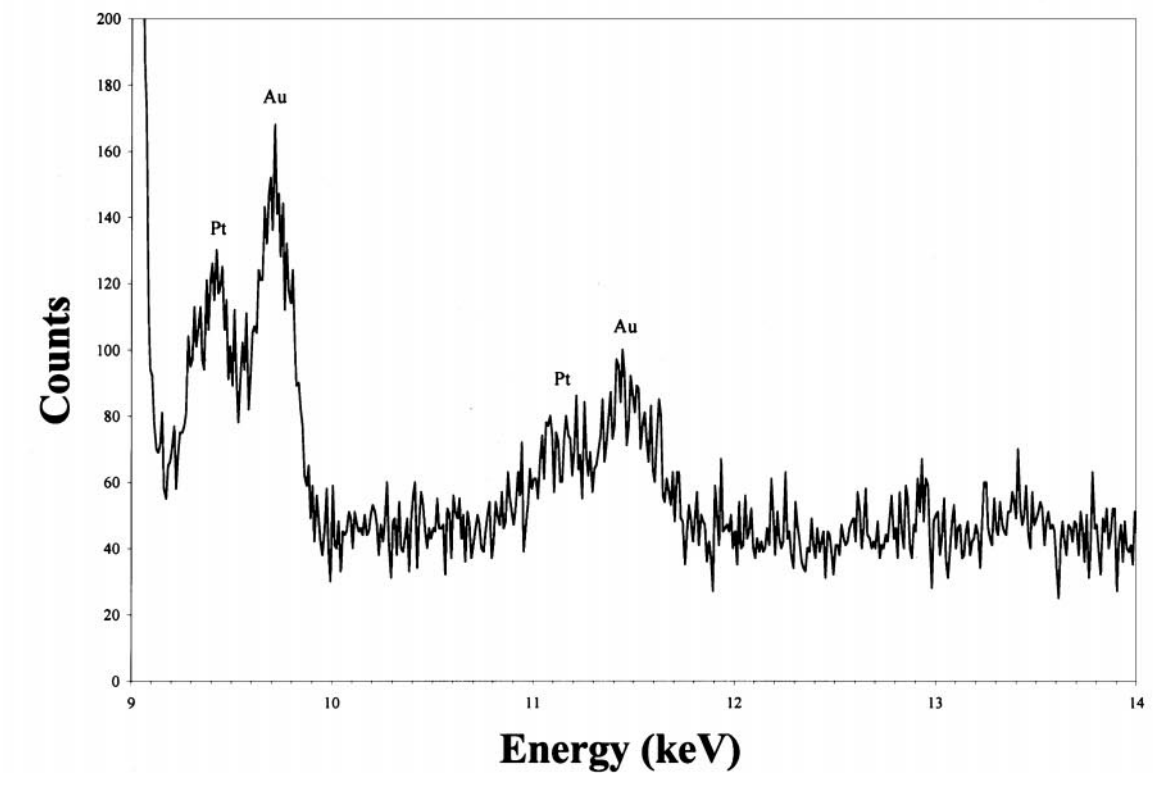

FIG. 6. Typical high-magnification micrograph and EDS spectrum (probe diameter ≈ 100 nm) of the 1-Pt_2Au_4 catalyst.

TABLE 1

CO Chemisorption Data

Catalyst	CO/Pt_{total}			$\nu(C{\equiv}O)$ cm^{-1}
	Total	Strong	% Weak	
1-Pt	0.49	0.44	8	2074
1-(Pt + 2Au)	0.46	0.42	9	2072
1-Pt_2Au_4	0.76	0.52	31	2125, 2063
0.15-Pt	0.52	0.45	13	2073
0.15-(Pt + 2Au)	0.79	0.68	14	2072
0.15-Pt_2Au_4	1.3	0.88	32	2125, 2063

Fourier transform (DRIFT) spectra of bound CO were recorded (Table 1, Fig. 7). Total CO uptakes at 60 Torr were determined by subtracting a blank silica CO uptake isotherm from the total measured CO uptake isotherm. The quantity of strongly bound CO was determined by measuring a second isotherm after evacuation; the weakly bound CO is the difference between the total and strongly bound CO. The designation of strongly bound CO is an arbitrary (42) one as all chemisorption is reversible (43). In this case, strongly bound CO has been designated as that which remains bound to the catalyst after 10 min of evacuation at room temperature with a diffusion pump ($P \approx 1–4 \times 10^{-7}$ Torr). Control experiments with the Au sample showed no strong CO adsorption; however, there was a small amount (<0.03 CO/Au_{total}) of weakly bound CO when the silica blank was subtracted. CO chemisorption data for the 0.15-Pt and 1-Pt catalysts were also used to calculate an average metal particle diameter using the Advanced Scientific Designs, Inc. Chemisorption Analysis Version 4.06 software package. Calculations were made from the total and strongly bound CO values and averaged. The average particle diameter for both the 0.15-Pt and the 1-Pt catalysts was calculated to be 3.6 nm.

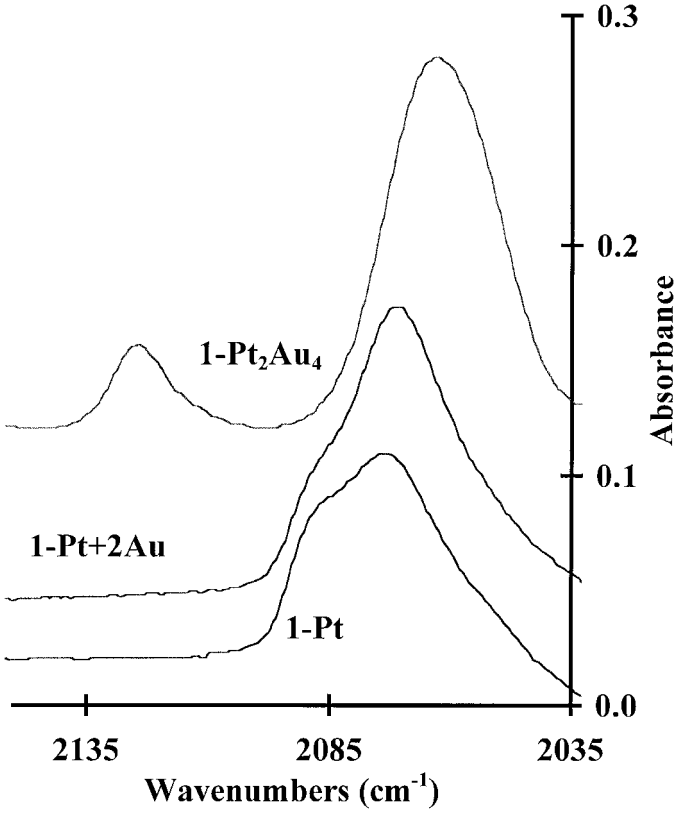

FIG. 7. DRIFT spectra of the C≡O stretching region for carbon monoxide adsorbed to the 1-Pt, 1-(Pt + 2Au), and 1-Pt_2Au_4 catalysts.

For the higher loaded 1-Pt and 1-(Pt + 2Au) catalysts, there are no major differences in CO binding characteristics, in terms of both total and strongly bound CO. The lower loaded 0.15-Pt catalyst has slightly higher CO chemisorption values than the 1-Pt catalyst; however, 0.15-(Pt + 2Au) binds considerably more CO than the other chloride salt-based catalysts. All of the wetness-impregnated catalysts have 85–90% of the total CO uptake as strongly bound CO, in agreement with previously reported CO chemisorption data for Pt–Au catalysts on silica (16). Catalysts prepared from the organometallic cluster have significant differences in CO adsorption compared with the wetness-impregnated catalysts. In both series of catalysts (1 and 0.15% Pt), the cluster-derived catalysts bind significantly more CO than either of the salt-based catalysts. For the 0.15-Pt_2Au_4 catalyst, the value for total CO uptake exceeds unity relative to the number of moles of Pt in the catalyst. An intriguing property of the cluster-derived catalysts is that they bind significantly less CO as evacuation time or temperature is increased. The original CO uptake isotherms can be regenerated by rereducing the catalyst at 200°C for 1 h. This behavior is observed only with the cluster-based catalysts.

The addition of Au via wetness coimpregnation has only a small effect on the DRIFT spectrum of adsorbed carbon monoxide (Table 1, Fig. 7), decreasing the C≡O stretch by about 2 cm^{-1}. Values of $\nu(C{\equiv}O)$ for the lower loaded catalysts (Table 1) were similar. The DRIFT spectra of both the 1-Pt_2Au_4 and 0.15-Pt_2Au_4 catalysts indicated a CO stretch that is red shifted about 12 wavenumbers relative to the Pt catalysts. In addition, the cluster-derived catalyst has a weak band at about 2124 cm^{-1} due to CO weakly bound to Au (16). A comparable band was not observed for the Au sample using the DRIFTS protocol described under Methods.

Hexane Conversion Catalysis

The hexane conversion reaction was chosen to evaluate the performance of the catalysts because a wide array of products can be formed (see below) and because platinum–gold catalysts have been extensively studied for this reaction (4–11). All experiments were run with the use of a microflow reactor thermostated at 400°C with a 1 : 16

TABLE 2

Catalyst Activity for Total Hexane Conversion[a]

Catalyst	Total activity[b]	TOF[c]
1-Pt	47 (5)	0.1
0.15-Pt	49 (5)	0.1
1-(Pt + 2Au)	45 (8)	0.1
0.15-(Pt + 2Au)	63 (9)	0.09
1-Pt_2Au_4	51 (5)	0.1
0.15-Pt_2Au_4	50 (7)	0.06

[a] Catalysis at 400°C and 16 : 1 H_2 : hexane ratio at ambient pressure.
[b] Activity in millimoles of hexane consumed per mole of Pt per second. Standard errors in the slope determined from least-squares analysis are in parentheses.
[c] Turnover frequency in moles of product per mole of surface Pt per second with standard errors in parentheses. For Pt and Pt + 2Au, the average of the weakly and strongly bound CO fractions was used to determine the fraction of available surface platinum. For Pt_2Au_4, only the strongly bound fraction of CO was used.

hexane : H_2 mixture at ambient pressure. Control experiments with blank silica and with Au showed no conversion of hexane under the reaction conditions. All catalyst activity measurements (Table 2) were made between 30 and 70 min on stream with total hexane conversions below 10%. Plots of conversion versus inverse space velocity were linear for conversions below 10% and were used to determine catalyst activity.

Catalyst selectivities (reported in mass percent) were calculated from the fraction of hexane converted to a given product classification divided by the total fraction of hexane converted. The major product classifications used hereafter are cracking (C_1–C_5 hydrocarbons), isomerization (2-methylpentane and 3-methylpentane), hexenes, methylcyclopentane (MCP), and 1,6-cyclization products (benzene and cyclohexane). No measurable production of dimethylbutanes was ever observed. For all of the catalysts, the ratio of 2-methylpentane (2-MP) to 3-methylpentane (3-MP) was found to be 2.0–2.1 for conversions between 5 and 15%. Selectivity-versus-conversion profiles for the 1% catalysts are shown in Figs. 8, 9, and 10. The profiles for the 0.15% loaded catalysts are similar and are not shown.

For all catalysts in this study, hexenes are the dominant product at very low conversion (<2%) and hexene selectivity rapidly drops as conversion increases. MCP is also rapidly produced at conversions below 10%; however, selectivity for MCP production increases with conversion, plateaus, and then decreases at high conversions (>20%). Simultaneously, selectivity for cracking, isomerization, and 1,6-cyclization products increases with conversion of hexane. The 1-Pt and 0.15-Pt catalysts are relatively unselective for any one product class. At conversions above 15% each of the product classes (except hexenes) ranges from

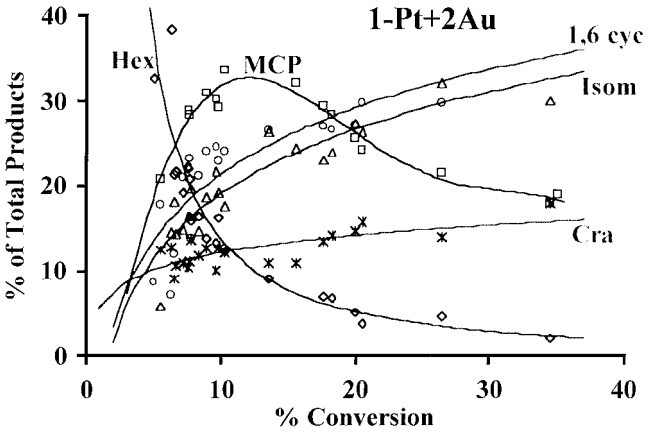

FIG. 9. Selectivity-versus-conversion profile for the 1-(Pt + 2Au) catalyst. Hex, hexenes; Iso, isomerization (2- and 3-methylpentane); MCP, methylcyclopentane; 1,6 cyc, 1,6-cyclization (benzene and cyclohexane); Cra, light hydrocarbons. Lines are drawn to help see the trends.

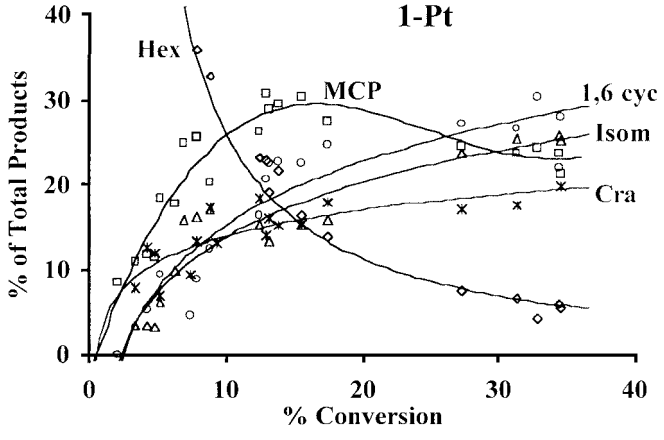

FIG. 8. Selectivity-versus-conversion profile for the 1-Pt catalyst. Hex, hexenes; Iso, isomerization (2- and 3-methylpentane); MCP, methylcyclopentane; 1,6 cyc, 1,6-cyclization (benzene and cyclohexane); Cra, light hydrocarbons. Lines are drawn to help see the trends.

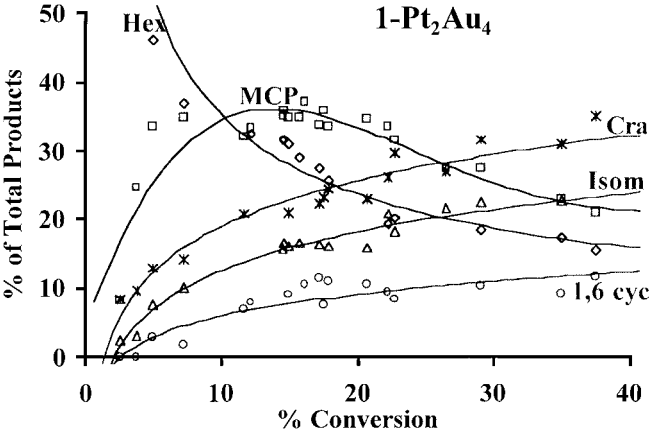

FIG. 10. Selectivity-versus-conversion profile for the 1-Pt_2Au_4 catalyst. Hex, hexenes; Iso, isomerization (2- and 3-methylpentane); MCP, methylcyclopentane; 1,6 cyc, 1,6-cyclization (benzene and cyclohexane); Cra, light hydrocarbons. Lines are drawn to help see the trends.

about 20 to 30% of the total products. The coimpregnation of Au with Pt in the 1-(Pt + 2Au) and 0.15-(Pt + 2Au) catalysts decreases selectivity toward cracking products and increases selectivity for 1,6-cyclization and isomerization products, in agreement with literature reports (9–11). The cluster-derived catalysts, on the other hand, have selectivities significantly different from that of either of the wetness impregnates catalysts. The 1-Pt_2Au_4 and 0.15-Pt_2Au_4 catalysts both have higher selectivity for cracking products and lower selectivity for 1,6-cyclization.

To make more meaningful selectivity comparisons between catalysts with different activities and dispersions, we have evaluated the rates of the cracking, 1,6-cyclization, 1,5-cyclization, and isomerization reactions on the lower (0.15% Pt) loaded catalysts. The 1,5-cyclization activity is the sum of production of MCP and methylpentanes as they are assumed to come from the same five-member ring surface intermediate (1). Similar to the plots for total catalyst activity, plots of production of a given product class versus inverse space velocity were prepared for each of the these four product classes. All of these plots were linear at conversions below 15% and their slopes give the specific activity of a catalyst for that class of reaction. This specific activity is the rate of production (in millimoles per second) of a given product class per mole of Pt in the catalyst. Data from the three 0.15% loaded catalysts are compiled in Table 3, which also includes rates corrected for Pt availability (TOFs).

There are significant differences in the distribution of cracking products from the cluster-derived catalysts relative to the catalysts prepared from salts, regardless of the catalyst loading. Figure 11 shows the molar light hydrocarbon distributions for the 1% loaded catalysts at 10% conversion. The distribution of light hydrocarbons does not change significantly at other conversions and there are no major differences between the cracking product distributions of the 1 and 0.15% loaded catalysts. The molar light hydrocarbon distributions for the chloride salt-based catalysts are very similar, with methane being the dominant product. For the cluster-derived catalyst, however, C_3 hydrocarbons are the predominant cracking product and the methane fraction is less than half of the methane fraction of the traditional catalysts. It is also noteworthy that, for all of the catalysts, there is relatively little production of isobutane or isopentane, the expected products of hydrogenolysis of 2- and 3-methylpentane (44–46). The production of isobutane and isopentane has previously been used as a measure of the extent of secondary reactions (44). The small quantities of these molecules indicate that the methylpentanes do not undergo further reaction at the conversions used in this study.

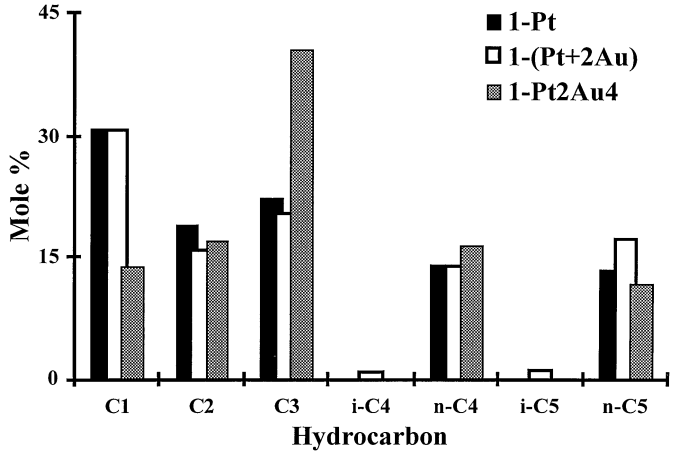

FIG. 11. Light hydrocarbon distributions at 10% conversion for the 1-Pt, 1-(Pt + 2Au), and 1-Pt_2Au_4 catalysts.

TABLE 3

Specific Activities of the 0.15% Loaded Catalysts

Product class	0.15-Pt	0.15-Pt + 2Au	0.15-Pt_2Au_4
	Catalyst activity[a]		
1,6-cyclization	14 (1)	19 (2)	6.6 (0.6)
Total MCP + MPs	25 (3)	35 (3)	24 (2)
Isomerization (2-MP + 3-MP)	9.3 (0.9)	12 (1)	7.8 (0.3)
Cracking	9.5 (0.7)	8 (1)	20 (1)
	Turnover frequency[b] × 10^3		
1,6-cyclization	29 (2)	26 (3)	8 (1)
Total MCP + MPs	51 (7)	48 (4)	27 (2)
Isomerization (2-MP + 3-MP)	19 (2)	16 (2)	9 (1)
Cracking	20 (1)	11 (2)	23 (2)

[a] Activity in millimoles of product per mole of Pt per second with standard errors in parentheses.

[b] Turnover Frequency in moles of product per mole of surface Pt per second with standard errors in parentheses. For Pt and Pt + 2Au, the average of the weakly and strongly bound CO fractions was used to determine the fraction of available surface platinum. For Pt_2Au_4, only the strongly bound fraction of CO was used.

The catalysts were also tested for their resistance to deactivation using initial conversions of ca. 10%. Plots for the 1% Pt catalysts are shown in Fig. 12; the 0.15% Pt catalysts are similar. The chloride salt-based catalysts have very similar deactivation properties and lose much of their activity within the first several hours of catalysis. After undergoing hexane conversion catalysis overnight, the activity observed for the traditional catalysts was primarily dehydrogenation activity; only a small fraction of the products after 10 h on stream were cracking, isomerization, or cyclization products. The bimetallic cluster, on the other hand, showed an initial small drop in activity but had significantly increased resistance to deactivation processes, retaining ca. 85% of its initial activity after 15 h on stream. Selectivities did not appreciably change during overnight catalysis runs for either of the cluster-based catalysts.

Because many alkane conversions are often considered to be hydrogen controlled, an attempt was made to evaluate the relative amounts of hydrogen on the surfaces of

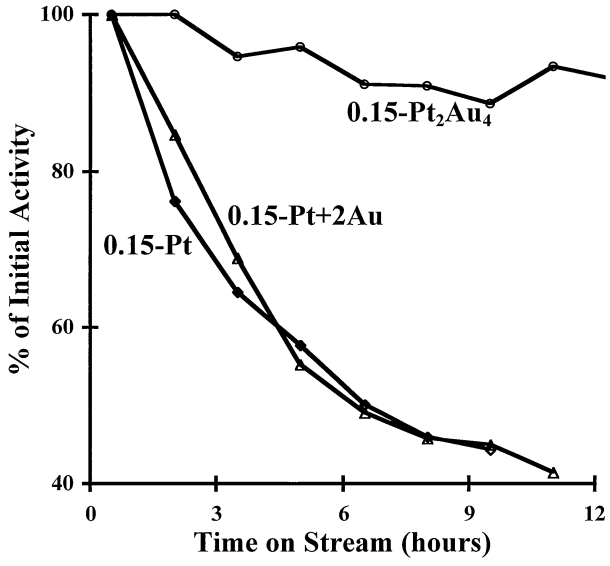

FIG. 12. Catalyst deactivation during hexane conversion catalysis for the 1-Pt, 1-(Pt + 2Au), and 1-Pt_2Au_4 catalysts. Catalyst masses were adjusted to so that initial conversion was ≈10% conversion of hexane.

the catalysts under the reaction conditions. One means of accomplishing this, suggested by Paál and co-workers (47, 48), is by examining the product ratio of MCP to total 1,5-cyclization products (MCP + MPs) from the reaction data. Plots of the the MCP/(MCP + MPs) ratio versus conversion for the 0.15% loaded catalysts are in Fig. 13. Over the entire conversion range studied, the cluster-derived catalyst always had a higher MCP/(MCP + MPs) value than the traditionally prepared catalysts, suggesting that there is less available surface hydrogen on the cluster-derived catalysts.

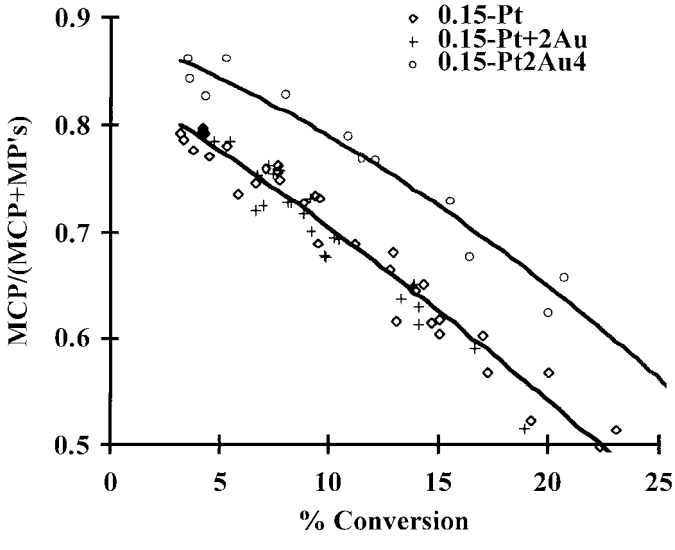

FIG. 13. MCP/(MCP + MPs) fraction versus conversion for the 0.15-Pt, 0.15-(Pt + 2Au), and 0.15-Pt_2Au_4 catalysts.

DISCUSSION

This study reports the first attempt to prepare supported Pt–Au catalysts from a bimetallic molecular precursor that does not contain phosphine ligands. Supported Pt and Pt–Au catalysts from chloride salts with the same Pt : Au ratio as in the $Pt_2Au_4(C{\equiv}C^tBu)_8$ cluster have been prepared and characterized. On the whole, with the activation conditions used in this study, there is relatively little evidence for interaction between Pt and Au when the catalyst is prepared by coimpregnating platinic and auric acids. Using the bimetallic cluster as the sole metal source yields a uniform bimetallic catalyst that is composed of small supported particles. Further, the particles prepared via this route have a unique morphology or phase and the resulting catalysts have significantly enhanced selectivity for producing lighter hydrocarbons from hexane. Despite this increased rate of C–C bond scission, the cluster-derived catalysts have vastly superior resistance to deactivation under the hexane conversion reaction conditions

Temperature-Programmed Reduction

To compare our results with those previously reported for supported Pt–Au catalysts and to examine activation procedures for the cluster-based catalysts, temperature-programmed reduction experiments were preformed both before and after the oxidation step of the standard activation protocol. TPR experiments on the supported chloride precursors reported here are in good qualitative agreement with those reported previously for supported Pt–Au catalysts (11). The addition of Au to Pt via wetness coimpregnation of chloride salts does not have a great effect on the hydrogen uptake profile of the supported precursors. The primary reduction peak is shifted roughly 50°C to higher temperatures and there is a small broad peak at slightly lower temperature than the reduction peak for Pt (Fig. 1). Similar such peaks have been attributed to the possible formation of a Pt–Au alloy in previous studies (11). The shift in reduction temperature of platinic acid might also be due to the presence of other ions on the support, rather than an interaction between Pt and Au. Similar shifts in the reduction temperature of hexachloroplatinate have been observed when the potassium salt is used (rather than the acid) as the metal precursor (49). Reduction of the cluster precursor produces a significantly larger hydrogen uptake peak (175–235°C) than is observed using chloride salts. The size of this peak is attributed to the destruction of the precursor acetylide ligands. Highly volatile ligand residues (e.g., methane) can pass through the dry ice/acetone trap (see Methods) and make quantitative interpretation of peak areas observed with the TCD detector impossible for the cluster-based catalysts.

There are important differences observed between the catalysts after the oxidation step (Fig. 2). The platinic acid

catalyst has two peaks (75 and 236°C) attributed to the reduction of a Pt oxide or oxychloride (41) and from unoxidized platinic acid, respectively. After the oxidation step, the TPR profile of the wetness-coimpregnated catalyst most resembles overlaying the reduction profiles of oxidized platinic acid and supported auric acid. It generally has the same features as oxidized platinic acid, although the Pt oxide/oxychloride peak is much smaller for the codeposited catalyst. We attribute the shoulder at 180°C on the primary reduction peak (unoxidized platinic acid) to the reduction of auric acid. The small peaks at higher temperatures (>300°C) in the profile of the coimpregnated catalyst are not present in the TPR profile of the platinic acid catalysts. We cannot rule out that these might arise from the formation of an alloy, but they may also be due to continuing reduction of auric acid.

The single reduction peak observed in the reduction profile of the cluster-derived catalyst is consistent with the reduction of an oxidized platinum species or a species with a platinum species of low coordination (49). There are no indications of intact cluster remaining on the support after the oxidation step of the standard activation protocol. This could possibly be caused by the lower initial oxidation states of the metals in the molecular precursor or to the nature of the cluster ligands. It is not appropriate to make strong conclusions about the ultimate catalyst based on TPR profiles. The TPR experiment is considerably different from the reduction step in the activation protocol and any conclusions drawn from these experiments may or may not have relevance to the real catalyst. Rather, these TPR experiments are being used to compare the relative homogeneity (or inhomogeneity) of the cluster-derived catalysts to the traditionally prepared catalysts and literature precedent and to look for obvious evidence of phase separation in the cluster-derived catalysts. When chloride salts are used as catalyst precursors, we see evidence for phase separation of Pt and Au after the oxidation step. This is not surprising given the large miscibility gap between the two metals and given that oxygen is well known to sinter metals on silica (1, 50–52). In addition, both chloride salt-based catalysts are relatively nonuniform, having both platinic acid and platinum oxide peaks. When the bimetallic cluster is used as the sole metal source, the oxidation step of the activation protocol yields a much more uniform catalyst in which there is no readily apparent segregation of the two metals.

Characterization of the Activated Catalysts

Platinic acid catalysts. Characterization data for the traditionally prepared 0.15-Pt and 1-Pt catalysts indicate that the only major difference between the catalysts is the amount of metal present. Particle size distribution histograms (Fig. 3), CO chemisorption data (Table 1), and the characteristic stretch of the C≡O bond for carbon monoxide adsorbed to the catalyst surface (Table 1) are all the same within the errors of the measurement for the two Pt catalysts. The DRIFT spectra of CO bound to the catalyst surfaces are in good agreement with other reports of Pt-based catalysts on silica (16, 53, 54). The observed values of ν(C≡O) for the 1-Pt and 0.15-Pt catalysts (2074 and 2073 cm^{-1}, respectively) are consistent with CO linearly adsorbed on Pt. The presence of bridging carbonyls was not detected on any of the catalysts in this study, the absence of which has been previously reported for Pt catalysts on silica (16, 53). The similarity of the DRIFTS, chemisorption, and TEM data for 1-Pt and 0.15-Pt suggests that the formation of Pt metal particles is not greatly affected by the percentage loading of metal. This conclusion is consistent with literature reports (1); at these loadings, metal dispersion is expected to be independent of metal loading (55) and Pt crystallite size is expected to be determined by the structure of the support (1).

For both of the Pt catalysts, some sintering and particle agglomeration have occurred. Most of the large imaged particles ($d > 15$ nm) were generally rectangular or peanut shaped, suggesting formation from two nearby smaller particles. Presumably, this particle growth is due to a combination of the deposition technique and the preoxidation of the catalyst. Sintering is known to be severe at elevated temperatures in the presence of oxygen, but less so in hydrogen (1, 50–52). Because particle size distributions did not change appreciably after several hours of hexane conversion catalysis (in hydrogen at 400°C), the hydrogen treatments used are much less likely to be the primary cause of the observed sintering.

The mean particle diameters calculated from TEM data for the Pt catalysts (4.5 nm) are in reasonable agreement with the average particle diameters calculated from CO chemisorption experiments (3.6 nm); however, the average particle diameters calculated from TEM experiments are somewhat larger. This implies that there are some smaller particles that are not adequately imaged with the instrument used. Because it is difficult to obtain good contrast between the metal particles and the support, small particles can only be imaged in very thin sections of the sample. Since the smallest particles are observable only in the thinnest sections of the TEM samples (rather than in the bulk of the samples), particle size distributions may slightly underestimate the contributions of these particles to the average particle diameter throughout the catalyst. A larger particle size discrepancy between microscopy and chemisorption data has been reported in a previous study of silica-supported Pt and Pt–Au catalysts (11). The discrepancy was similarly attributed to nonnormal size distributions observed by TEM in which the observation of a few large particles substantially increased the average particle diameter calculated from micrographs. Hence, microscopy data provide a general framework of what types of particles might be present in the catalyst and approximate the relative

numbers of those particles. This highlights the importance of comparing microscopy data with bulk characterization data (such as chemisorption) to obtain an accurate representation of the catalyst as a whole.

Coimpregnated chloride catalysts. Results for the coimpregnated 1-(Pt + 2Au) and 0.15-(Pt + 2Au) catalysts (Fig. 4) indicate that, relative to the monometallic Pt catalysts, metal particle size is more dependent on the metal loading. Omitted from the histograms for these catalysts are some exceptionally large particles, often with dimensions exceeding 100 nm. Particles of this size are pure Au (or highly enriched in Au to the point where Pt is undetectable) and are comparable to the dimensions of the pores on the support. This is an indication that Au is highly mobile on the support and may be able to completely fill some of the pores. This mobility is presumably caused by the oxidation step in the standard catalyst activation protocol (see above). The histograms for these catalysts are also somewhat misleading because the composition of individual particles is unknown. For the 1-(Pt + 2Au) catalyst, Pt dispersion measured by CO chemisorption is only slightly lower than for the 1-Pt catalyst, suggesting that the larger particles contain primarily Au and the smaller particles are primarily Pt. As with the monometallic Pt catalysts, the contribution of the smallest particles is probably underrepresented by the histograms.

These observations and conclusions also apply to the 0.15-(Pt + 2Au) catalysts; however, there is an important difference in the CO chemisorption data. This catalyst has significantly more Pt available for CO binding than the other chloride salt catalysts (Table 1). One possible cause is that the smaller particles observed are bimetallic in nature and have significant amounts of surface Pt. This is unlikely for a traditionally coimpregnated catalyst because Au-rich alloy surface compositions have lower workfunctions than Pt-rich alloys or pure Pt (18). Consequently, alloys of Pt and Au would be expected to be surface enriched in Au rather than Pt (18). Surface composition of Pt–Au alloys is known to change with adsorption of CO, however, and it cannot be ruled out that the addition of CO could bring Pt to the surface of small alloy particles. A second, more plausible explanation for the differences in CO chemisorption is that the presence of Au affects Pt particle size by preventing larger Pt particles from forming. The energy-dispersive spectra collected during TEM experiments and particularly the catalysis results (see below) tend to argue in favor of the latter explanation. Energy-dispersive spectra varied widely from region to region but, in general, Pt was observed primarily in regions containing the smallest particles and Au was present when larger particles were imaged. Some of the variation might also be attributed to the metal concentrations and EDS count rates used in the study and to the fact that Pt and Au have closely overlapping peaks.

The similarity of the DRIFTS and catalysis data for the 1-(Pt + 2Au) and 0.15-(Pt + 2Au) catalysts also suggests that the active particles are very similar for the two coimpregnated catalysts, despite the lower dispersion of the former. The presence of Au in the coimpregnated Pt + 2Au catalysts causes no measurable increase in the amount of weakly bound CO that could be attributed to CO bound to Au and there is no evidence for CO adsorbed to Au in the DRIFT spectra of these catalysts. One possible explanation is that, in the 1-(Pt + 2Au) catalyst, Au is coating some Pt, rendering a large portion of the active metal inaccessible to substrate molecules.

The presence of active (non-"cherry pit") bimetallic particles certainly cannot be excluded on the basis of the TEM and chemisorption data; however, no strong evidence was found to suggest that there are important interactions between the two metals for the chloride salt-based catalysts. In previous studies of silica-supported Pt–Au catalysts prepared from platinic and auric acids, bimetallic particles have been characterized with high-resolution electron microscopy and EDS (11). In these studies, the authors examined Pt-rich catalysts (1% Pt coimpregnated with 0.3 and 0.7% Au) on a nonporous silica and concluded that bimetallic particles were formed with one of the coimpregnated catalysts but not the other. Since such relatively small differences in Au loading may determine whether or not bimetallic particles are formed, it is not surprising that no strong evidence for bimetallic particles is found with a much higher Au loading (2%). In addition to having a much more porous support than in the above study, activation conditions in this study include a high-temperature (300°C) oxidation step. Similar to the results reported here for the coimpregnated catalysts, Sachdev and Schwank also observed a wide range of particle sizes with varying degrees of Pt–Au interaction (11) and the authors succinctly highlighted the complexities of these samples and the difficulty of preparing bimetallic Pt–Au particle catalysts.

Cluster-derived catalysts. Using the bimetallic cluster as the sole metal source yields a catalyst with much more uniform and highly dispersed particles than either the mono- or bimetallic catalysts prepared via wetness impregnation methods. The micrograph in Fig. 6 is typical of the samples imaged and the histograms in Fig. 5 show very few particles larger than 3.5 nm. Additionally, the exceptionally large ($d \approx 100$ nm) Au particles that are present in the traditionally prepared bimetallic catalyst were not observed for these samples. Micrographs of the Pt_2Au_4 catalysts contain a few larger particles (5–20 nm) that probably form during the oxidation portion of the standard activation protocol (see above). Histograms of the catalysts do not change appreciably after several hours of hexane conversion catalysis (400°C with flowing hydrogen), so sintering processes under hydrogen do not appear to be important for the cluster-derived catalysts.

Chemisorption data support the TEM data, with large values of strongly bound CO indicating high Pt dispersion

(Table 1). The cluster-derived catalysts have significantly larger weak CO uptakes than the traditionally prepared catalysts. The 1-Pt_2Au_4 catalyst has somewhat lower CO uptakes than the 0.15-Pt_2Au_4 catalyst, despite having a nearly identical particle size distribution. This could be due to the inability to image some very small particles in the lower loaded catalyst, but it may also result from the longer evacuation time required for the higher loaded catalyst to achieve the base pressure used in the chemisorption experiments.

DRIFT spectra of the Pt_2Au_4 catalysts (Table 1, Fig. 7) show that the C≡O stretch for linearly bound Pt-C≡O is red shifted 10–12 cm^{-1} relative to the chloride-based catalysts; a new band at 2124 cm^{-1} is also observed. This 2124 cm^{-1} band, which is due to CO weakly bound to Au (16), is of particular interest because it is strong evidence for intimate contact between Pt and Au in the Pt_2Au_4 catalysts. The presence of this band clearly indicates that the large CO uptakes by the cluster-derived catalysts (>1 CO per Pt) are due to CO weakly bound to Au. When the cluster is used as the metal source, some CO is adsorbed to Au and bound strongly enough to remain after the nitrogen purge. Two possible motifs for CO binding to Au support this model. A very small ($d \approx$ 10-20 Å) mono- or bimetallic particle would be expected to have surface Au atoms with low coordination numbers and therefore might be able to bind CO. In such a particle, Au could conceivably bind CO directly or it could be bound to the particle on Pt sites and quickly migrate or "spillover" to Au atoms.

The shift in the stretching frequency of carbon monoxide bound to the cluster-derived catalysts is also consistent with the formation of very small bimetallic particles. A variety of electronic, geometric, and particle size arguments have been previously invoked to explain shifts of this magnitude (12 cm^{-1}) in the CO stretch for both alloys and supported metal particle catalysts (8, 56, 57). An integral part of these arguments is the contribution of dipole coupling between adsorbed CO molecules on a metal particle. Briefly, as the surface becomes saturated with CO, the characteristic ν(C≡O) blue shifts as coupling between the adsorbed dipoles (CO molecules) increases. Hence, smaller particles and particles in which Pt is diluted by Au (geometric effect) would both be expected to have red-shifted C≡O stretches. Additionally, there is the possibility of an electronic effect. Increased surface electron density would increase the back-donation of electron density from Pt to antibonding C≡O orbitals, thus weakening the C≡O bond and red-shifting ν(C≡O) (58). Increased electron density at the surface of the particles could be due to the exposure of different crystallographic planes (56) or possibly to an electronic donation from Au to Pt. These dipole coupling, geometric, and electronic effects depend greatly on surface coverage of the adsorbate and cannot be properly evaluated and discussed without a careful surface coverage study (56). Such a study is currently underway for this and the analogous Pt–Cu system, the results of which will be the subject of a later publication (59).

Hexane Conversion Catalysis

Table 2 shows the activities of the catalysts for conversion of hexane to products. All activity measurements were made between 30 and 70 min on stream. The relative activities of the chloride catalysts are generally consistent with Pt dispersion measured by CO chemisorption. It is interesting that the two cluster-derived catalysts have nearly identical total activities despite having different carbon monoxide uptakes. Given that the particle size distributions for these two catalysts are also nearly identical, the activity data support the conclusion that the lower CO uptakes by the 1-Pt_2Au_4 catalyst result from the evacuation immediately prior to the chemisorption experiment (see above).

Results for all the catalysts (Tables 2 and 3, Figs. 8–13) are generally consistent with standard models for alkane reforming by metals (1). The trends in hexane selectivity (initial production of olefins followed by a rapid decrease in hexene selectivity) observed for all of the catalysts are consistent with a rapid equilibrium in which olefin production is under thermodynamic control. We have provided a more detailed explanation of this argument and included calculations using these experimental reaction conditions in a previous publication (37) and do not repeat them here. Similar calculations and the conclusion of a thermodynamically equilibrated dehydrogenation of hexane were also recently reported (44).

Methylcyclopentane is also rapidly produced at conversions below 10%; however, selectivity for MCP production increases with conversion, plateaus, and then decreases at high conversions (>20%). Simultaneously, selectivity toward cracking, isomerization, and 1,6-cyclization products increases with conversion of hexane. The production of methylpentanes is consistent with the cyclic mechanism (rather than the bond shift mechanism) in which the substrate molecule undergoes 1,5-cyclization to form a five-membered ring intermediate on the metal surface. This intermediate can then desorb, yielding MCP, or further react by ring opening to yield 2-MP or 3-MP (1, 5, 60). The contributions of the two mechanisms cannot be definitively evaluated without proper labeling studies (5, 60); however, this conclusion as to the dominance of the cyclic mechanism is strongly supported by the observed 2-MP/3-MP ratio which was always close to the statistical value of 2 expected for this mechanism.

The selectivity profiles for the traditional wetness-impregnated catalysts shown in Figs. 8 and 9 are also consistent with this mechanism. Figure 8 shows that the platinum catalyst 1-Pt is relatively unselective for any one product class. This observation is also supported by the specific activity

data for the 0.15-Pt catalyst (Table 3), in which production rates for cracking, isomerization, and 1,6-cyclization products are similar. Measurement of the rate of MCP production in the same manner as was used for the other product classes was not possible because plots of MCP fraction versus inverse space velocity were not linear. This is consistent with the selectivity-versus-conversion profiles and the previously described mechanism in which MCP production is linked to methylpentane production. Therefore, the total of MCP + MPs was used to estimate the total rate of 1,5-cyclization and included the result as one of the specific activities in Table 3. In doing this, the following assumptions have been made based on the cyclic mechanism for hexane isomerization described above: (1) the bond shift mechanism does not appreciably account for the production of 2-MP and 3-MP by these catalysts (1); (2) ring enlargement, i.e., conversion of MCP to cyclohexane or benzene, is not a viable reaction pathway (48); and (3) further reaction of MCP or methylpentanes (e.g., cracking) does not appreciably occur. The last assumption is supported by the lack of significant production of isopentane or isobutane by any of the catalysts (44–46).

The selectivity profile for the 1-(Pt + 2Au) catalyst in Fig. 9 indicates that the coimpregnation of Au with Pt decreases selectivity for cracking reactions. The data for the 0.15-(Pt + 2Au) catalyst (Table 3) also indicates that the production of light hydrocarbons is slower than the skeletal rearrangement processes (1,6-cyclization, MCP and MP production via 1,5-cyclization) or reforming reactions. Further, when the specific activity data are corrected for Pt dispersion (TOF data), there is essentially no difference in the rates of these skeletal rearrangements on the 0.15-Pt and 0.15-(Pt + 2Au) catalysts. The rate of production of light hydrocarbons, on the other hand, decreases by about 45%. These results are consistent with a previously described model for Au affecting Pt particle size. Studies with supported Pt on silica and single-crystal studies with Pt–Au alloys suggest that hydrogenolysis (terminal C–C bond scission cleavage to yield methane) reactions are structurally demanding and require the largest ensemble sizes (1). If the average Pt particle size decreases from the coimpregnation of Au, the reactions requiring the largest ensembles (terminal hydrogenolysis) would be most affected and those reactions requiring smaller ensembles (1,5- and 1,6-cyclization) would be less affected. The catalysis results here suggest that Pt particles formed in the presence of Au are not small enough to have a significant effect on these less demanding reactions. The importance of particle surface morphology in determining catalyst selectivity should also be stressed. Work by Somorjai and co-workers has shown that, for both pure Pt and Pt–Au annealed alloy catalysts, changing the Pt crystallographic plane has large effects on product selectivity for hexane reforming reactions (8–10). Hence, differences in catalyst selectivity might also be partially attributed to differing distributions of surface planes as particle sizes and morphologies change.

The catalysts prepared from the bimetallic $Pt_2Au_4(C{\equiv}C^tBu)_8$ cluster have the opposite effect of adding Au via traditional coimpregnation. The selectivity profile in Fig. 10 (1-Pt_2Au_4) shows enhanced selectivity for the production of light hydrocarbons relative to 1-Pt. In contrast, the coimpregnation of Au with Pt from chloride salts decreased selectivity for light hydrocarbon production. The turnover frequencies from the specific activity data (Table 3) show that this shift in selectivity is not due to a significant enhancement in the rate of light hydrocarbon production by the 0.15-Pt_2Au_4 catalyst. Rather, the 1,5-cyclization, isomerization, and 1,6-cyclization processes are much slower on the cluster-derived catalysts than on the traditional chloride-based catalysts.

The data from the cracking product distributions (Fig. 11) suggest that the mechanism of cracking is very different for the traditional versus cluster-derived catalysts. Product distributions for the 1-Pt and 1-(Pt + 2Au) catalysts show a large propensity for methane production, with >30% (by moles) of the light hydrocarbons being methane. For this to occur, successive terminal carbon abstraction (hydrogenolysis) reactions must be occurring on the adsorbed substrate. These reactions most likely occur on the largest platinum particles that are present in the traditionally prepared catalysts (1). On these particles, once the hydrocarbon is bound (probably in an end on fashion) and C–C bond fission occurs, the molecule continues to react via this terminal carbon abstraction mechanism. The lack of production of isobutane and isopentane (Fig. 11) indicates that these hydrogenolysis processes do not occur as further reactions of 2-MP or 3-MP (44–46). If the conclusion is drawn from the absence of isobutane and isopentane that further reactions of MCP and MPs are negligible, then the high production of methane (relative to the other light hydrocarbons) must be due to consecutive terminal carbon abstraction events on individual substrate molecules on at least some of the metal particles.

The light hydrocarbon distribution for the 1-Pt_2Au_4 catalyst (Fig. 11), on the other hand, is fairly symmetric about the production of C_3 hydrocarbons; i.e., the mole fraction of methane is roughly the same as that of *n*-pentane and the mole fraction of ethane is roughly the same as the mole fraction of butane. In addition, the cluster-derived catalysts have a slight propensity for C–C bond fission near the center of the molecule rather than at the C_1–C_2 bond, in good agreement with literature reports for nonhydrogenolytic cracking by Pt (1). This indicates that cracking reactions occurring on the cluster-based catalysts are single C–C bond fission events and that the successive terminal carbon abstractions (hydrogenolysis) that occur on the chloride-based catalysts are not major contributors to the overall light hydrocarbon production. This suggests that, on the

cluster-derived catalysts, the C_6 hydrocarbon is bound with the adsorbing C–C bond parallel to the surface (as opposed to an end-on adsorption for the traditional catalysts) and that, after the initial C–C bond rupture, there is not a great deal of further bond fission. This change is mechanism is also consistent with the reduced activity for 1,6-cyclization. Several studies on various monofunctional supported Pt catalysts, especially on basic zeolites, have correlated benzene production with increased terminal hydrogenolysis and attributed both to end-on adsorption sites (44, 61, 62).

Because the light hydrocarbon distributions are different for 0.15-Pt and 0.15-Pt_2Au_4, the similarity in the corrected rates of light hydrocarbon production between the two may be coincidence. It is noteworthy, however, that the enhanced cracking selectivity by Pt_2Au_4 catalysts is in direct contrast to the diminished hydrogenolysis selectivity observed when Au is coimpregnated with Pt in the Pt + 2Au catalysts. This may be due to the formation of a unique metal particle morphology from the organometallic metal source. Further, the reduction in the specific rates for the other product classes suggests that this unique morphology might be characterized by having very small Pt ensembles or even "isolated" Pt atoms surrounded by Au. This conclusion is also consistent with the previously mentioned particle size and ensemble effect arguments for Pt catalysts and Pt–Au alloys in which isomerization, cyclization, and (terminal) hydrogenolysis reactions are all considered to be structure sensitive. It may not be possible to make a strong correlation between the Pt_2Au_4 catalysts and single-crystal work, however. For Pt–Au alloy crystal surfaces, both activity and selectivity depend greatly on both the exposed crystallographic plane and the Au content. Although the results for the Pt_2Au_4 catalysts are generally consistent with some previous studies of supported Pt catalyst and single-crystal work, the properties of these new catalysts may be unique to a particle morphology that is not attainable by methods other than the decomposition of the organometallic cluster.

It is interesting and perhaps somewhat counterintuitive that the cluster-derived catalysts, which favor cracking reactions, have greatly improved resistance to deactivation, as shown in Fig. 12. Given the shift away from terminal hydrogenolysis for the cluster-derived catalysts, it is possible that polyunsaturated coke precursors may not be able to form on the surface of the Pt_2Au_4 catalysts. Another possibility suggested by the observation of CO weakly bound to Au in the DRIFT spectra of the Pt_2Au_4 catalysts is that the Au provides additional sites for the transfer of carbonaceous deposits or for storing hydrogen. Given the rich chemistry of dihydrogen activation by molecular (ligand stabilized) Pt–Au cluster compounds in solution and in the solid state (30, 33, 63), it seems likely that hydrogen would be partially transferred to the Au in these new cluster-derived particle catalysts. This might provide additional and readily available surface hydrogen to rapidly hydrogenate coke precursors.

One means of evaluating surface hydrogen under the reaction conditions, suggested by Paál and co-workers (47, 48), is by examining the ratio of MCP to total 1,5-cyclization products (MCP + MPs). Briefly, Paál and co-workers' argument is that this fraction of MCP is determined by the available surface hydrogen. When more surface hydrogen is available under catalysis conditions, greater production of methylpentanes is expected because the conversion of MCP to 2- or 3-methylpentane requires 2 eq of H. Thus, as the production of methylpentanes increases, the MCP/(MCP + MPs) ratio is expected to decrease. This fraction is shown over a wide range of conversions in Fig. 13. Surprisingly, the Pt_2Au_4 catalysts have a larger value for this ratio over the entire conversion range, implying that there is actually less surface hydrogen available on the cluster-derived catalysts. This conclusion is supported by hydrogen chemisorption results that indicate reduced hydrogen uptakes (relative to CO uptakes) for cluster-derived catalysts (64). This result is also consistent with slower rates of cyclization and isomerization by the cluster-derived catalysts as these reactions (kinetically) require hydrogen to occur (47). In the case of small Pt clusters prepared on various zeolite supports, the MCP/(MCP + MPs) ratio has also been correlated with the electron richness of the metal surface, measured by ν(C≡O) of CO bound to the catalyst surface (44); the higher MCP/(MCP + MPs) fraction for the cluster-derived catalysts does indeed correlate to a lower C≡O stretching frequency. This suggests that the red shift may be due to an electronic effect or to the preparation of a more electron-rich surface when the cluster is used. The greatly improved resistance to deactivation appears to arise from the unique morphology (including its electronic and geometric properties) that is prepared when the $Pt_2Au_4(C{\equiv}C^tBu)_8$ cluster is used as the catalyst precursor.

Often associated with the possible effects of differing amounts of surface hydrogen, differences in quantities and types of surface carbon may be important in determining the catalytic properties of the different catalysts. Surface carbon is well known to affect hydrocarbon reactions on metal surfaces (2, 60, 65), and the composition and quantity of surface carbon are often controlled by hydrogen (47). One possibility is that the particle morphology prepared using the cluster precursors slows the deposition of carbon or alters the carbon deposited during hexane conversion catalysis. Consequently, differences in catalysis between the traditional and cluster-derived catalysts might also be partially attributed to differences in the quantity and type of adsorbates on the metal surfaces (e.g., hydrogen, carbon) during catalysis.

Another conceivable cause of the differences between the traditionally prepared and cluster-derived catalysts is the presence or absence of chloride in the resulting catalysts.

The presence of chloride has been shown to have significant effects on hydrocarbon conversion catalysis; however, these effects are often associated with the strengthening of acid sites used in the bifunctional mechanism (2) rather than catalysis by metals. Further, the relatively small differences between the Pt and Pt + 2Au catalysts argue against residual chloride being the primary factor in determining catalytic properties for the chloride-containing catalysts. The traditionally prepared Au-containing catalysts have more than twice the chloride content (prior to activation) of the monometallic Pt catalysts, yet there are only small differences in catalytic results (decreased hydrogenolysis activity, Table 2). If the bifunctional mechanism becomes important with additional chloride, enhanced activity for several reactions (particularly isomerization), would be expected as would significant production of dimethylbutanes (2). These effects are not observed for the chloride-containing catalysts; however, it cannot be ruled out that some of the differences between the traditional and cluster-derived catalysts partially result from the presence of residual chloride in the standard catalysts.

SUMMARY

This article describes the preparation and characterization of Pt–Au catalysts prepared by adsorption and thermal decomposition of bimetallic molecular clusters. Using the $Pt_2Au_4(C{\equiv}C^tBu)_8$ cluster, small and uniform bimetallic Pt–Au particles have been prepared. These particles are outside of the normal bulk miscibility range for Pt–Au alloys and have high Pt dispersions. These new particles have a unique morphology that was not attainable via traditional impregnation methods with chloride salts and comparable activation conditions. This unique morphology appears to have an electron-rich bimetallic surface in which both Pt and Au are able to participate in the binding of substrates such as carbon monoxide.

In catalytic testing with the hexane conversion reaction, the new catalysts were found to have high activity for the production of light hydrocarbons. This result is in striking contrast to the diminished production of light hydrocarbons found when Au was coimpregnated with Pt using chloride salts. This shift in selectivity coicides with a shift in the distribution of light hydrocarbons. The traditionally prepared catalysts produce methane as the dominant light hydrocarbon by successive terminal carbon abstractions of some substrate molecules. The cluster-derived catalysts catalyze only one C–C bond scission event per substrate molecule. Further, the particles formed using this method have greatly enhanced resistance to deactivation during hexane conversion catalysis, despite greater selectivity for light hydrocarbon production. These differences in catalysis may result from the unique particle size, composition, and morphology that arise from the intimate contact between the two metals when the bimetallic cluster is used as the metal source.

ACKNOWLEDGMENTS

This research was funded by a grant from the University of Minnesota Graduate School. Alex Schabel was a participant in a NSF–REU program in the Department of Chemistry at the University of Minnesota.

REFERENCES

1. Gates, B. C., Katzer, J. R., and Schuit, G. C. A., "Chemistry of Catalytic Processes." McGraw–Hill, New York, 1979.
2. Ponec, V., and Bond, G. C., *in* "Catalysis by Metals and Alloys" (B. Delmon and J. T. Yates, Eds.), Studies in Surface Science and Catalysis, Vol. 95. Elsevier, Amsterdam, 1995.
3. Clarke, J. K. A., and Taylor, J. F., *J. Chem. Soc. Faraday Trans.* **71**, 2063 (1975).
4. Kane, A. F., and Clarke, J. K. A., *J. Chem. Soc. Faraday Trans.* **76**, 1640 (1980).
5. O'Cinneide, A., and Gault, F. G., *J. Catal.* **37**, 311 (1974).
6. van Shaik, J. R. H., Dessing, R. P., and Ponec, V., *J. Catal.* **38**, 273 (1975).
7. Clarke, J. K. A., Manninger, I., and Baird, T., *J. Catal.* **54**, 230 (1978).
8. Sachtler, J. W. A., and Somorjai, G. A., *J. Catal.* **81**, 77 (1983).
9. Sachtler, J. W. A., and Somorjai, G. A., *J. Catal.* **89**, 35 (1984).
10. Yates, R. C., and Somorjai, G. A., *J. Catal.* **103**, 208 (1987).
11. Sachdev, A., and Schwank, J., *J. Catal.* **120**, 353 (1989).
12. Sachtler, J. W. A., Biberian, J. P., and Somorjai, G. A., *Surf. Sci.* **110**, 43 (1981).
13. Lam, Y. L., and Boudart, M., *J. Catal.* **50**, 530 (1977).
14. Menezo, J. C., Denanot, M. F., Peyrovi, S., and Barbier, J., *Appl. Catal.* **15**, 353 (1985).
15. Barbier, J., Marecot, P., Mabilon, G., Durant, D., and Prigent, M., French Patent 90/15,750 (1990).
16. Balakrishnan, K., Sachdev, A., and Schwank, J., *J. Catal.* **121**, 441 (1990).
17. Dumas, J. M., Geron, C., Hadrane, H., Marecot, P., and Barbier, J., *J. Mol. Catal.* **77**, 87 (1992).
18. Bouwman, R., and Sachtler, W. H. M., *J. Catal.* **19**, 127 (1970).
19. Anderson, J. R., and Mainwaring, D. E., *J. Catal.* **35**, 162 (1974).
20. Anderson, J. R., Elmes, P. S., Howe, R. F., and Mainwaring, D. E., *J. Catal.* **50**, 508 (1977).
21. Iwasawa, Y., and Yamada, M., *J. Chem. Soc. Chem. Commun.*, 675 (1985).
22. Gates, B. C., Guczi, L., and Knozinger, H., *in* "Metal Clusters in Catalysis" (B. Delmon and J. T. Yates, Eds.), Studies in Surface Science and Catalysis, Vol. 29. Elsevier, Amsterdam, 1986.
23. Xiao, F. S., and Ichikawa, M., *Cuihua Xuebao* **14**, 87 (1993).
24. Kawi, S., Xu, Z., and Gates, B. C., *Inorg. Chem.* **33**, 503 (1994).
25. Kawi, S., Alexeev, O., Shelef, M., and Gates, B. C., *J. Phys. Chem.* **99**, 6926 (1995).
26. Ugo, R., Dossi, C., and Psaro, R., *J. Mol. Catal. A* **107**, 13 (1996).
27. Deutsch, S. E., Xiao, F. S., and Gates, B. C., *J. Catal.* **170**, 161 (1997).
28. Zhao, A., and Gates, B. C., *J. Catal.* **168**, 60 (1997).
29. Alexeev, O., Panjabi, G., and Gates, B. C., *J. Catal.* **173**, 196 (1998).
30. Pignolet, L. H., Aubart, M. A., Craighead, K. L., Gould, R. A. T., Krogstad, D. A., and Wiley, J. S., *Coord. Chem. Rev.* **143**, 219 (1995).
31. Pignolet, L. H., *in* "Catalysis by Di- and Polynuclear Metal Cluster Complexes" (R. D. Adams and F. A. Cotton, Eds.). VCH, New York, 1997.
32. Pignolet, L. H., and Krogstad, D. A., *in* "Gold: Progress in Chemistry, Biochemistry and Technology" (H. Schmidbauer, Ed.). Wiley, Chichester, 1998.

33. Graf, I. V. G., Bacon, J. W., Curley, M. E., Ito, L. N., and Pignolet, L. H., *Inorg. Chem*. **35**, 689 (1996).
34. Graf, I. V. G., Ph.D. thesis, University of Minnesota, Minneapolis, 1996.
35. Yuan, Y., Asakura, K., Wan, H., Tsai, K., and Iwasawa, Y., *Chem. Lett.*, 129 (1996).
36. Chandler, B. D., Schabel, A., and Pignolet, L. H., *in* "Catalysis of Organic Reactions" (F. E. Herkes, Ed.), p. 607. Marcel Dekker, New York, 1998.
37. Chandler, B. D., Rubinstein, L. I., and Pignolet, L. H., *J. Mol. Catal.* **133**, 267 (1998).
38. Espinet, P., Fornies, J., Martinez, F., Tomas, M., Lalinde, E., Moreno, M. T., Ruiz, A., and Welch, A. J., *J. Chem. Soc. Dalton Trans.*, 791 (1990).
39. Giedt, D. C., and Nyman, C. J., *Inorg. Synth.* **8**, 239 (1966).
40. Lemaitre, J. L., Menon, P. G., and Delannay, F., *in* "Chemical Industry Series: Characterization of Heterogeneous Catalysts" (F. Delannay, Ed.), Vol. 15, p. 316. Marcel Dekker, New York, 1984.
41. Delmon, B., *in* "Handbook of Heterogeneous Catalysis" (G. Ertl, H. Knozinger, and J. Weitkamp, Eds.), Vol. 1, p. 264. VCH, Weinheim, 1997.
42. Che, M., and Bennett, C., *Advances in Catalysis* **36**, 55 (1989).
43. Kip, B. J., Duivenvoorder, F. B. M., Koningsberger, D. C., and Prins, R., *J. Catal.* **105**, 26 (1987).
44. Menacherry, P. V., and Maller, G. L., *J. Catal.* **177**, 175 (1998).
45. Leclercq, G., Leclercq, L., and Maurel, R., *J. Catal.* **50**, 87 (1977).
46. Garin, F., Aeiyach, S., Legare, P., and Maire, G., *J. Catal.* **77**, 323 (1982).
47. Paál, Z., *in* "Hydrogen Effects in Catalysis" (Z. Paál and P. G. Menon, Eds.). Dekker, New York, 1988.
48. Paál, Z., Zhan, Z., Manninger, I., and Sachtler, W. M. H., *J. Catal.* **155**, 43 (1995).
49. Hurst, N. W., Gentry, S. J., and Jones, A., *Catal. Rev. Sci. Eng.* **24**, 233 (1982).
50. Benesi, H. A., Curtis, R. M., and Studer, H. P., *J. Catal.* **10**, 328 (1968).
51. Boudart, M., Aldag, A. W., Ptak, L. D., and Benson, J. E., *J. Catal.* **11**, 35 (1968).
52. Spenandel, L., and Boudart, M., *J. Phys. Chem*. **64**, 204 (1960).
53. Bartok, M., Sarkany, J., and Sitkei, A., *J. Catal.* **72**, 236 (1981).
54. Haaland, J. L., *Surf. Sci.* **185**, 1 (1987).
55. Dorling, T. A., Lynch, B. W. L., and Moss, R. L., *J. Catal.* **20**, 190 (1971).
56. Hollins, P., *Surf. Sci. Rep.* **16**, 51 (1992).
57. Lane, G. S. T, M. J., Modica, F. S., and Barr, M. K., *J. Catal.* 465 (1993).
58. van Santen, R. A., *J. Chem. Soc. Faraday Trans. I* **83**, 1915 (1987).
59. Chandler, B. D., and Pignolet, L. H., manuscript in preparation (1999).
60. Anderson, J. R., *Adv. Catal.* **23**, 1 (1973).
61. Tauster, S. J., and Steger, J. J., *J. Mater. Res. Soc. Symp. Proc.* **111**, 419 (1988).
62. Mielczarski, E., Hong, S. B., Davis, R. J., and Davis, M. E., *J. Catal.* **134**, 359 (1992).
63. Rubinstein, L. I., and Pignolet, L. H., *Inorg. Chem*. **35**, 6755 (1996).
64. Chandler, B. D., Ph.D. thesis, University of Minnesota, Minneapolis, 1999.
65. Gault, F. G., *Adv. Catal.* **30**, 1 (1981).